Intelligent Service Robotics (2021) 14:519–534
https://doi.org/10.1007/s11370-021-00373-8

ORIGINAL RESEARCH PAPER

Power assistance algorithm of an E-Trike for older adults based on inverse dynamics

Tuani de Sa Rosa[1] · **Jung-Yup Kim**[1]

Received: 30 October 2020 / Accepted: 16 June 2021 / Published online: 19 July 2021

Abstract
Maintaining a regular physical activity routine can promote healthy and successful aging. The use of power assist electric bicycles (e-bikes) has been shown to be a good exercise option since it allows older adults to adjust the degree of physical activity while maintaining higher levels of enjoyment compared to riding conventional bicycles. However, their use may present a fall risk to older adults due to their inherent instability and it is difficult to determine suitable power assistance from motor. We seek to solve this problem by using an electric trike (e-trike) instead of an e-bike and propose two novel power assistance algorithms to determine the assistive torque for our developed e-trike. Inverse dynamics calculations using pedal force, pedal angle, and crank angle are performed for effective assistance. The first algorithm is aimed at older adults with weak lower body muscle strength by analyzing the rear wheel torque, and the second is a joint assistive algorithm that reduces the physical effort for a specific leg joint (hip, knee, or ankle), for those who have joint problems, based on inverse dynamics. Finally, in a controlled environment, an experimental validation successfully verified the performance of the power assistance algorithms. Muscle activity in each test method is also presented using electromyography (EMG) to demonstrate the assistive performance of the muscles.

Keywords E-trike · Power assistance · Inverse dynamics · Older adults

1 Introduction

1.1 Background and motivation

The main source of air pollution in towns and cities is road transport. More than half of nitrogen oxide, carbon monoxide, and volatile organic compound emissions in urban areas come from road traffic [1]. Electric vehicles can be considered a promising technology in terms of addressing the above-mentioned issues since there is no oil usage or CO_2 emissions, on a per-km basis [2]. However, lack of physical activity of the passengers [3], and excessive use of public spaces for parking usage are some of the disadvantages of individual car usage, be it electric or not [4]. Using a conventional bicycle or an electric-assisted bicycle (e-bike) is a good solution to these problems, and particularly the latter for long distances or uphill segments. E-bikes further offer the advantage that they allow the rider to easily adjust the physical activity while maintaining higher levels of enjoyment compared to conventional bicycles [5].

On the other hand, for older adults, maintaining a regular physical activity routine is shown to beneficially affect brain function and executive cognitive processes [6]. Also, including physical fitness, and specifically muscular strength work, in daily physical activities is important since it can promote healthy and successful aging [7]. The use of e-bikes allows the user to cover longer distances than walking and requires less physical effort compared to regular bicycles, while still providing a beneficial exercise alternative for older adults [8]. As a result, older e-bike cyclists experience a rewarding feeling that, in turn, encourages more cycling time [8, 9].

When dealing with dual-task conditions, older adults exhibit abnormalities in temporal and spatial parameters of gait [10]. Furthermore, a reduction in gait speed due to reduced executive functions, memory, or attention can increase the fall risk [11]. Bicycling is a usable mode of transportation but is a source of severe injury among the elderly population [12]. Therefore, we selected a recumbent

✉ Jung-Yup Kim
jyk76@seoultech.ac.kr

[1] Department of Mechanical System Design Engineering, Seoul National University of Science and Technology, Seoul, South Korea 01811

trike (Fig. 1) as a test platform to maintain the advantages of the e-bike while removing the fall risk stemming from the required balance ability and studied effective power assistance algorithms for older adults.

1.2 Problem statement

Joint-related diseases, such as osteoarthritis and a decrease in muscle strength, are problems commonly seen among the elderly population [13, 14]. Performing a safe and effective physical activity is proven to increase muscle strength and power, improve physical function and reduce joint-related pain [15–17]. Another study has shown that, during cycling, the human body generates and directs power to the bicycle crank through its muscles in a coordinated and systematic way [18]. By analyzing the body configuration and human cycling dynamics, it is possible to investigate and determine the patterns of muscle movement and joint torques [19–21].

A problem is that conventional e-bikes do not consider the dynamics and joint torque pattern of the cyclist during cycling. Furthermore, conventional crank torque sensors cannot independently measure the pedal forces of both legs, and the joint torque pattern of each leg is not calculated accurately. Therefore, cyclist-specific assistance is not possible.

1.3 Related works

In terms of related works, various approaches to adapt and improve the e-bike system to provide a safe and efficient means of transportation while still being an effective exercise have been proposed. Guarisco et al. [22] proposed a control strategy for a dual-motor bicycle with regenerative braking to improve battery autonomy and lifetime, and they used the crank speed and torque sensor to determine the electric current that needs to be applied to each motor. Abagnale et al. [23] studied the assistance of pedaling, but instead of the motor being located in one of the bicycle wheel hubs, an electric motor was situated in a central position attached to the frame of the e-bike and transmitted the power to the pedal shaft. Lee et al. [24] proposed an enhanced fuzzy-logic-based control approach with a user-adaptive mechanism to online adjust the fuzzy parameters for power-assisted regulation to ensure riding comfort and safety. Abhilash et al. [25] proposed a gradient sensor-based throttle controller to control the e-bike. Huang et al. [26] used an observer-based sensor fusion algorithm to control the torque of the motor instead of using a torque sensor. These studies have not considered the specific joint torque reduction using inverse dynamics.

Fig. 1 ICE recumbent trike model Sprint X

1.4 Scope and contribution

This paper proposes novel power assistance algorithms using the crank position, pedal forces, and pedal angle information to determine the motor assistive torque for our developed electric trike instead of using a conventional crank torque sensor. This feature enables us to calculate the independent crank torques for the right and left pedal motions, which is significant for our algorithms. Hence, compared to other studies, it is possible to calculate the accurate joint torques of each leg independently through inverse dynamics of the lower body, and estimate accurate rear-wheel torque contributed by the rider during cycling. This means that the proposed algorithms can generate the variable motor assistive torque according to the joint torques and rear-wheel torque in real-time.

In this paper, two types of assistive methods are presented. The first is rear-wheel torque assistance for older adults with weak lower body muscle strength and the second is a leg joint assistive algorithm that reduces the physical effort for a specific leg joint (hip, knee, or ankle), based on inverse dynamics, for elderly people with joint problems.

1.5 Organization

This paper comprises six chapters. Chapter 2 presents the hardware design of our system, describing the smart pedal, actuator, and control system to build our e-trike test platform. Chapter 3 describes the human cycling dynamics which is required to calculate joint torques of each leg. In Chapter 4, the two types of assistance strategies are proposed in detail. To validate the proposed algorithms, the experiment setup, experimental results, and discussions are presented in Chapter 5. Finally, Chapter 6 concludes this paper with future works.

2 Hardware design

For our study, the ICE recumbent trike model Sprint X shown in Fig. 1 was modified into a power-assisted e-trike with minimum alterations to its original frame. The original

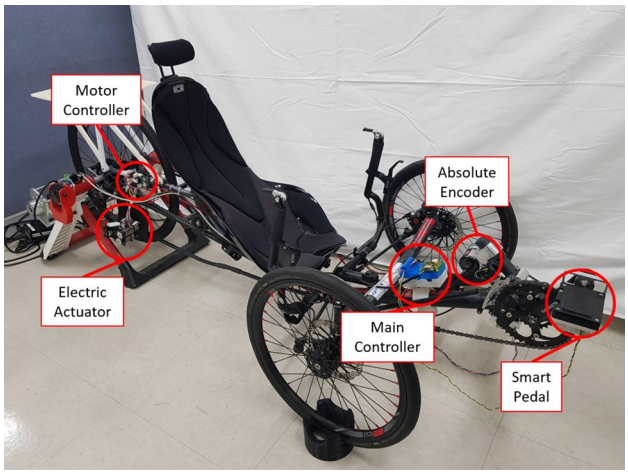

Fig. 2 Power-assisted trike developed in this study

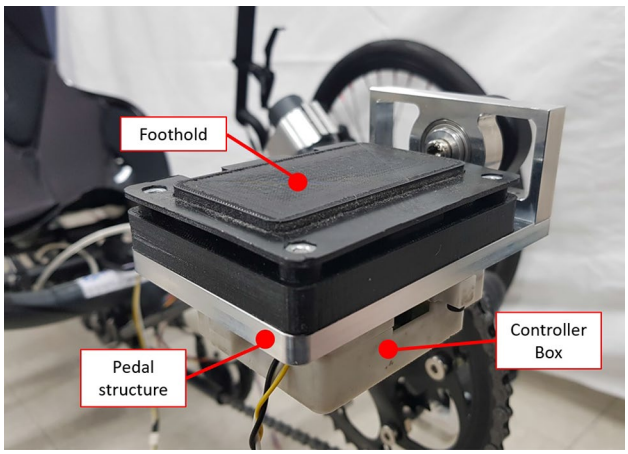

Fig. 3 Smart Pedal

pedals were substituted with smart pedals, which were developed in this study, and the actuator support structure was attached to the back of the trike's frame. The main controller and absolute encoder were attached to the front part of the frame, as shown in Fig. 2.

2.1 Smart pedal design

The smart pedal (Fig. 3) was designed to measure the inclination and the normal force of the pedal during cycling. These data are used to calculate the human cycling dynamics, the crank torque, and the rear-wheel torque of the e-trike. Pedal support structures were made of aluminum, and the controller box and foothold parts were made of PLA. Those materials were selected for both the lightweight structure and high friction of the foothold.

An Arduino Micro, which is small and lightweight, was used to collect the data from FSR sensors and an IMU sensor

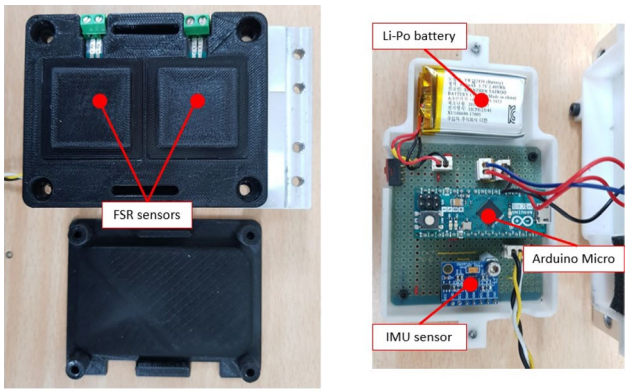

(a) Inside foothold **(b)** Inside controller box

Fig. 4 Inside of the Smart pedal

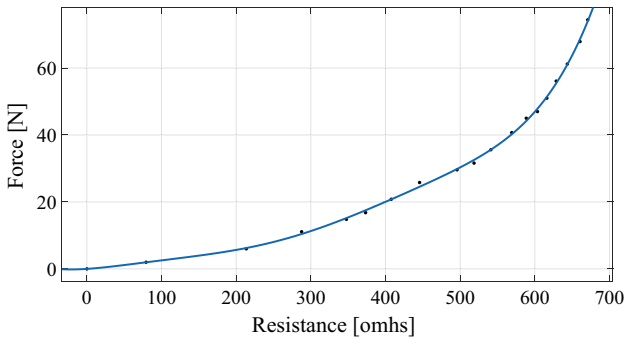

Fig. 5 Force sensor calibration

at a frequency of 300 Hz. The circuit is located inside the controller box that is attached to the lower part of the pedal. To power the Arduino Micro, two Li-Po batteries were used (Fig. 4).

Two FSR sensors were used on each pedal to measure the normal pedal force during cycling. Its maximum sensing force is 100 N; two FSR sensors of each pedal can thus measure max. 200 N. For our experimental setup, because the normal force does not reach values higher than 160 N, two FSR sensors are suitable. When the cyclist pushes the upper part of the pedal, the force is distributed to two square-shaped parts that are located over the sensing area of the FSR sensor, and hence the normal force is the sum of the two sensor outputs. The calibration of the FSR sensor was done using MATLAB. Known loads from 200 g to 8 kg were placed over the sensor and the output resistance values, r_s, of the sensor were collected, as shown in Fig. 5. Using the MATLAB Curve Fitting Toolbox, a conversion equation was finally created to find the force F_s in newtons as follows:

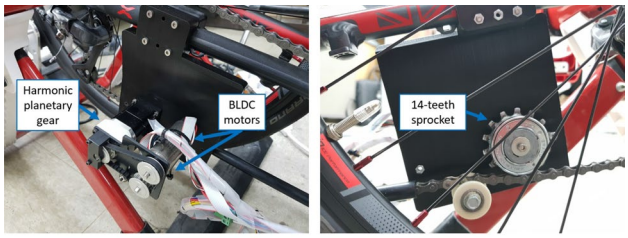

(a) Front view **(b)** Back view

Fig. 6 Electric actuator design

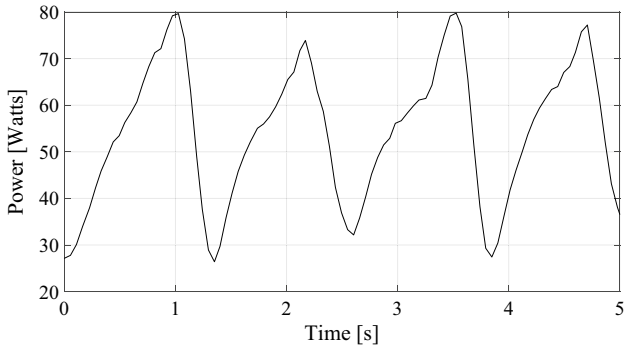

Fig. 7 Power trajectory of the rear wheel at avg. speed of 40 km/h

$$F_s = 1486 - 1883\cos\left(0.002336\, r_s\right) - 1231\sin\left(0.002336\, r_s\right) + 356.7\cos\left(0.004672\, r_s\right) + 883.1\sin\left(0.004672\, r_s\right) + 40.22\cos\left(0.007008\, r_s\right) - 176.3\sin\left(0.007008\, r_s\right) \quad (1)$$

2.2 Electric actuator design

The actuator that assists the cyclist during pedaling is composed of a 200 W BLDC motor, a 100 W BLDC motor, a harmonic planetary gear, and a 14 teeth sprocket that is attached to the trike chain (Fig. 6). The harmonic planetary gear has a reduction ratio of 30:1. The 100 W motor was not currently used for this study, but it was added to the system for further studies. The actuation system is used to assist the muscle power of the pilot during cycling; the motor was thus selected by considering that the actuator has to supply at least double the necessary power to move the trike on level ground at an avg. speed of 40 km/h (Fig. 7).

2.3 Control system design

The control system is composed of the main controller, an absolute rotary encoder, two smart pedals, the electric actuator, and an EPOS4 Maxon motor controller that controls the torque of the motor. Table 1 shows its detailed specifications.

The role of the main controller is to collect the data from the sensors and send the proper torque commands to the motor controller. More specifically, the Arduino Mega, which is used as the main controller, calculates human cycling dynamics and the necessary torque of the motor at a frequency of 200 Hz through the sensory data such as the crank angle, obtained from the absolute encoder, and the pedal force and angle acquired from the smart pedal (Fig. 8).

3 Human cycling dynamics

Solving the lower-body dynamics during the cycling motion of our trike system is essential, because it allows us to calculate the joint torques and joint powers of the hip, knee, and ankle joints through pedal force, pedal angle, and crank angle. These results are used to determine motor torque provided by the actuation system for the joint torque assistance.

3.1 3-Link planar mechanism

The dynamic analysis is performed by modeling the lower body as a 3-link planar mechanism, where the end point is moving along a circular pedal path while cycling, as shown in Fig. 9. The lengths of each linkage of the lower body and the crank arm are considered as constants. Considering the hip joint as the origin of the base coordinate frame, the joint

Table 1 Specifications of the control system

Item	Model	Specification
Main controller	Arduino Mega 2560	Clock speed 16 MHz
Motor controller	Maxon motor EPOS4 50/15 CAN	Max. output current 30A
BLDC motor	Maxon 48 V EC-4pole 30	200 W Power
Absolute encoder	EP50S8-1024-2R-P-5	1024 Divisions per rev
Pedal controller	Arduino Micro	Clock Speed 16 MHz
Force sensor	SEN0296	Force measuring range 0.2 N – 100 N
IMU sensor	MPU-6050	Gyroscope range ± 250°/sec
		Acceleration range ± 2 g

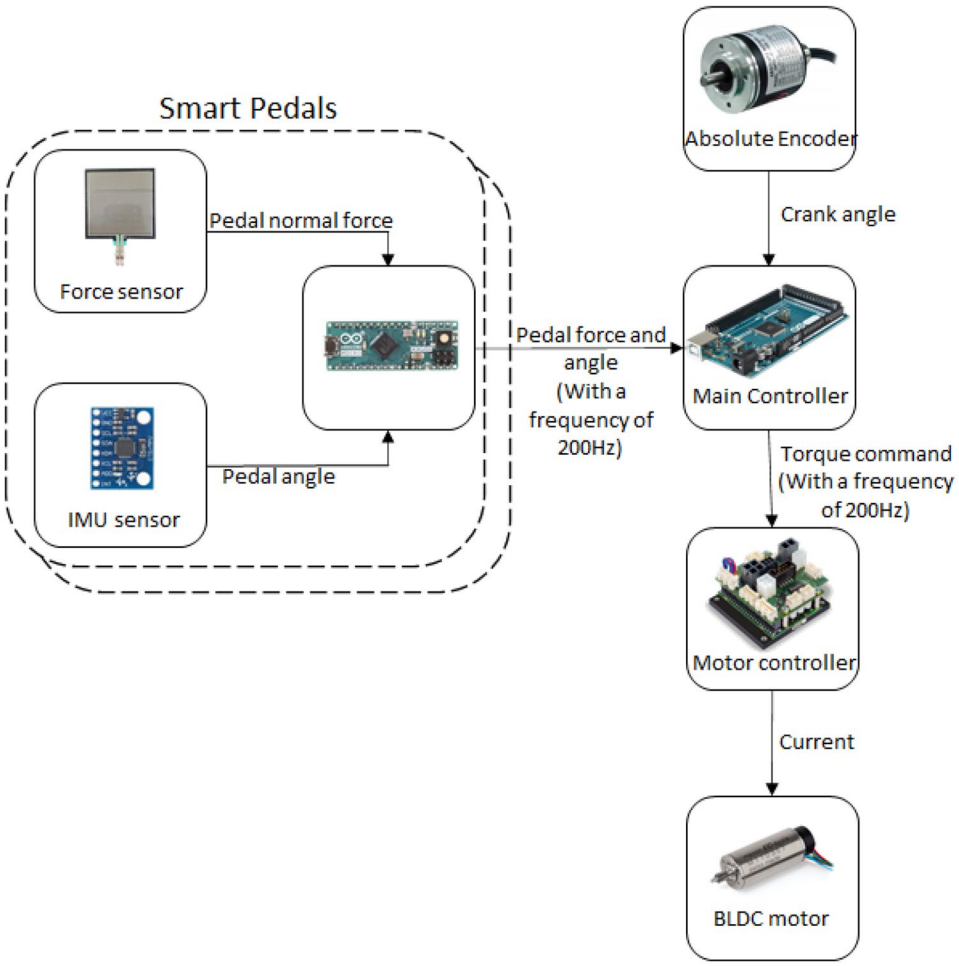

Fig. 8 Control system block diagram

angles are kinematically calculated from the pedal angle, which is equivalent to the foot inclination and the ankle position (Fig. 10a). Inverse kinematic equations are presented in Eqs. (2)-(7), where θ_1 is the hip angle, θ_2 is the knee angle, θ_3 is the ankle angle, α is the pedal angle with respect to the horizontal axis,δ is the crank angle with respect to the vertical axis, L_1, L_2 and L_3 are, respectively, the thigh, calf, and foot lengths, x_a and y_a are the ankle position, and x_p and y_p are the pedal position on the circular pedal path.

$$\theta_1 = atan2\left(y_a, x_a\right) - atan2\left(L_2 \sin\theta_2,\ L_1 + L_2\cos\theta_2\right) \tag{2}$$

$$\theta_2 = atan2\left(-\sqrt{1-\cos^2\theta_2}, \cos\theta_2\right) \tag{3}$$

$$\cos\theta_2 = \frac{x_a^2 + y_a^2 - L_1^2 - L_2^2}{2L_1L_2} \tag{4}$$

$$\theta_3 = \alpha - \theta_1 - \theta_2 \tag{5}$$

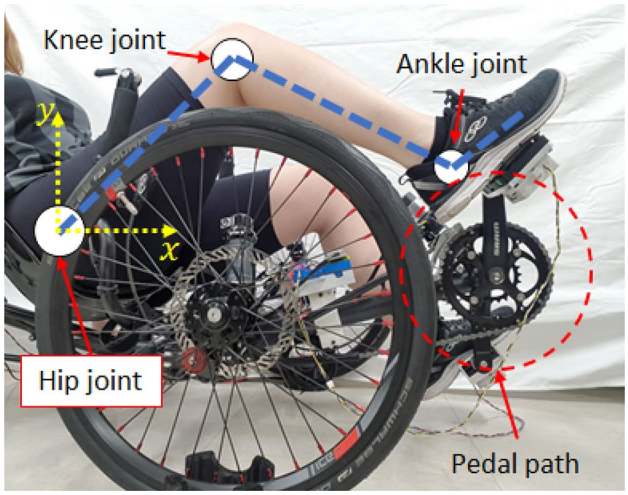

Fig. 9 3-link planar mechanism for analyzing human lower limbs

$$\begin{cases} x_p = 600 + r\sin\delta \\ y_p = r\cos\delta \end{cases} \tag{6}$$

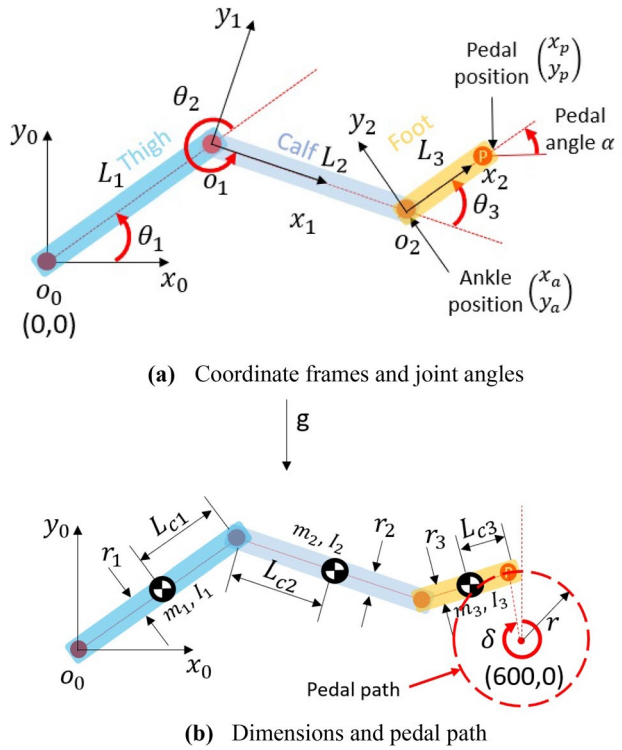

Fig. 10 Kinematic configuration of the 3-link planar mechanism

$$\begin{cases} x_a = x_p - L_3 \cos\alpha \\ y_a = y_p - L_3 \sin\alpha \end{cases} \tag{7}$$

The circular pedal path with a diameter of 340 mm has its center located at (600, 0) [mm] in relation to the origin. For calculation purposes, each link is considered as a rectangular prism and has its center of gravity in the middle of the link (Fig. 10b). Equation 8 gives the mass moment of inertia (I_i) for the rectangular prism. m_1, m_2, and m_3 are, respectively, the thigh, calf, and foot mass, and L_{ci} is half of L_i. Link length, width, and mass were obtained from the test subject, as shown in Table 2.

$$I_i = \frac{1}{12} m_i \left(r_i^2 + L_i^2\right) \tag{8}$$

3.2 Joint torque due to cycling motion

To perform the cycling motion, human joints require torque and power. The relation between motion and torque can be derived through the rigid-body dynamics and the joint torque and power can be calculated using Eq. (9).

$$M(\theta)\ddot{\theta} + C\left(\theta, \dot{\theta}\right)\dot{\theta} + G(\theta) = \tau \tag{9}$$

Table 2 Test subject information and parameters of the 3-link planar mechanism

Test Subject (One of the authors)	
Height [m]	1.64
Weight [kg]	62
Age [years]	29
Parameters	
L_1[m]	0.4
L_2[m]	0.39
L_3[m]	0.07
m_1[kg]	6.5
m_2[kg]	2.7
m_3[kg]	0.75
r[m]	0.17
r_1[m]	0.15
r_2[m]	0.1
r_3[m]	0.05

$$\begin{bmatrix} M_{11} & M_{12} & M_{13} \\ M_{21} & M_{22} & M_{23} \\ M_{31} & M_{32} & M_{33} \end{bmatrix} \begin{pmatrix} \ddot{\theta}_1 \\ \ddot{\theta}_2 \\ \ddot{\theta}_3 \end{pmatrix} + \begin{bmatrix} A_{112}\dot{\theta}_1\dot{\theta}_2 + A_{123}\dot{\theta}_2\dot{\theta}_3 + A_{113}\dot{\theta}_1\dot{\theta}_3 + A_{122}\dot{\theta}_2^2 + A_{133}\dot{\theta}_3^3 \\ A_{211}\dot{\theta}_1^2 + A_{233}\dot{\theta}_3^2 + A_{212}\dot{\theta}_1\dot{\theta}_2 + A_{223}\dot{\theta}_2\dot{\theta}_3 + A_{213}\dot{\theta}_1\dot{\theta}_3 \\ A_{311}\dot{\theta}_1^2 + A_{322}\dot{\theta}_2^2 + A_{312}\dot{\theta}_1\dot{\theta}_2 + A_{323}\dot{\theta}_2\dot{\theta}_3 + A_{313}\dot{\theta}_1\dot{\theta}_3 \end{bmatrix} + \begin{bmatrix} G_1 \\ G_2 \\ G_3 \end{bmatrix} = \begin{bmatrix} \tau_1 \\ \tau_2 \\ \tau_3 \end{bmatrix} \tag{10}$$

where,

$$M_{11} = m_1 L_{c1}^2 + I_1 + m_2 L_1^2 + \ + m_2 L_{c2}^2 + 2m_2 L_1 L_{c2} c_2 + I_2 + \ m_3 L_1^2 + m_3 L_2^2 + m_3 L_{c3}^2 + 2m_3 L_1 L_2 c_2 + \ 2m_3 L_2 L_{c3} c_3 + 2m_3 L_1 L_{c3} c_{23} + I_3 \tag{11}$$

$$M_{12} = m_2 L_{c2}^2 + m_2 L_1 L_{c2} c_2 + I_2 + m_3 L_2^2 + m_3 L_{c3}^2 + \ m_3 L_1 L_2 c_2 + 2m_3 L_2 L_{c3} c_3 + m_3 L_1 L_{c3} c_{23} + I_3 \tag{12}$$

$$M_{13} = m_3 L_{c3}^2 + m_3 L_2 L_{c3} c_3 + m_3 L_1 L_{c3} c_{23} + I_3 \tag{13}$$

$$M_{21} = m_2 L_{c2}^2 + I_3 + m_2 L_1 L_{c2} c_2 + I_2 + m_3 L_2^2 + m_3 L_{c3}^2 + \ m_3 L_1 L_2 c_2 + 2m_3 L_2 L_{c3} c_3 + m_3 L_1 L_{c3} c_{23} \tag{14}$$

$$M_{22} = m_2 L_{c2}^2 + I_3 + I_2 + m_3 L_2^2 + m_3 L_{c3}^2 + 2m_3 L_2 L_{c3} c_3 \tag{15}$$

$$M_{23} = m_3 L_{c3}^2 + m_3 L_2 L_{c3} c_3 + I_3 \tag{16}$$

$$M_{31} = m_3 L_{c3}^2 + m_3 L_2 L_{c3} c_3 + m_3 L_1 L_{c3} c_{23} + I_3 \quad (17)$$

$$M_{32} = m_3 L_{c3}^2 + m_3 L_2 L_{c3} c_3 + I_3 \quad (18)$$

$$M_{33} = m_3 L_{c3}^2 + I_3 \quad (19)$$

$$A_{112} = -2m_2 L_1 L_{c2} s_2 - 2m_3 L_1 L_2 s_2 - 2m_3 L_1 L_{c3} s_{23} \quad (20)$$

$$A_{123} = -2m_3 L_2 L_{c3} s_3 - 2m_3 L_1 L_{c3} s_{23} \quad (21)$$

$$A_{113} = -2m_3 L_2 L_{c3} s_3 - 2m_3 L_1 L_{c3} s_{23} \quad (22)$$

$$A_{122} = -2m_2 L_1 L_{c2} s_2 - m_3 L_1 L_2 s_2 - m_3 L_1 L_{c3} s_{23} \quad (23)$$

$$A_{133} = -m_3 L_1 L_{c3} s_{23} - m_3 L_2 L_{c3} s_3 \quad (24)$$

$$A_{211} = m_2 L_1 L_{c2} s_2 + m_3 L_1 L_2 s_2 + m_3 L_1 L_{c3} s_{23} \quad (25)$$

$$A_{233} = -L_1 L_{c3} m_3 c_{23} + L_1 L_{c3} m_3 s_{23} \quad (26)$$

$$A_{223} = 0 \quad (27)$$

$$A_{213} = -L_1 L_{c3} m_3 c_{23} - 2m_3 L_2 L_{c3} s_3 + L_1 L_{c3} m_3 s_{23} \quad (28)$$

$$A_{311} = m_3 L_2 L_{c3} s_3 + m_3 L_1 L_{c3} s_{23} \quad (29)$$

$$A_{322} = m_3 L_2 L_{c3} s_3 \quad (30)$$

$$A_{312} = 2m_3 L_2 L_{c3} s_3 \quad (31)$$

$$A_{323} = 0 \quad (32)$$

$$A_{313} = 0 \quad (33)$$

$$G_1 = m_1 g L_{c1} c_1 + m_2 g\left(L_1 c_1 + L_{c2} c_{12}\right) + m_3 g\left(L_1 c_1 + L_2 c_{12} + L_{c3} c_{123}\right) \quad (34)$$

$$G_2 = m_2 g L_{c2} c_{12} + m_3 g\left(L_2 c_{12} + L_{c3} c_{123}\right) \quad (35)$$

$$G_3 = m_3 g L_{c3} c_{123} \quad (36)$$

In Eq. (9) θ, $\dot{\theta}$, and $\ddot{\theta}$ are, respectively, the joint angle, joint velocity, and joint acceleration vectors, $M(\theta)$ is the inertia matrix, $C(\theta,\dot{\theta})$ is the centrifugal and Coriolis matrix, $G(\theta)$ is the gravity matrix, and τ is the joint torque vector. Equation (10) is the detailed form of rigid-body dynamics of our 3-link planar mechanism (Fig. 10).

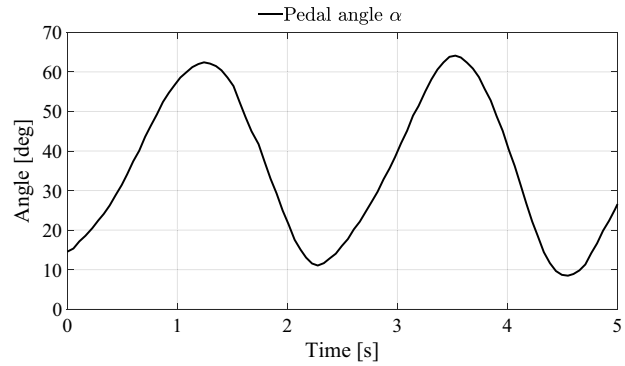

(a) Pedal angle

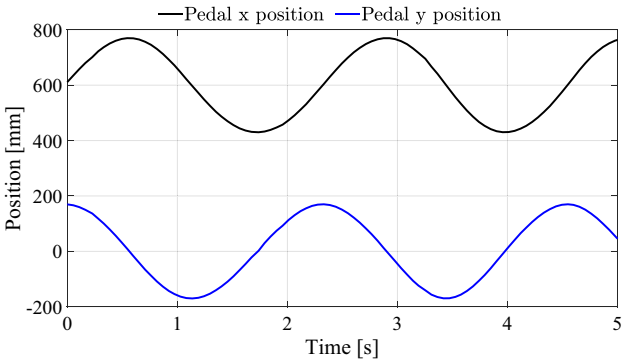

(b) Pedal position

Fig. 11 Pedal data used to calculate joint torque and power

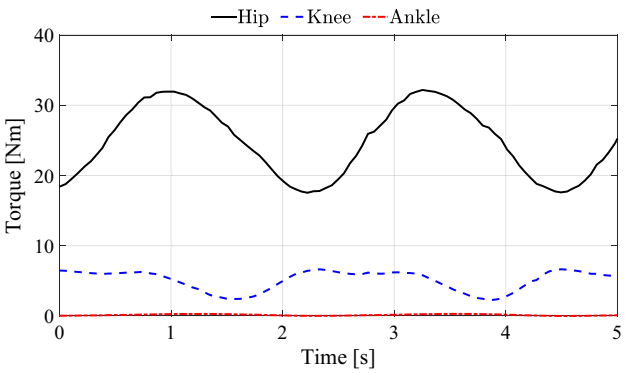

Fig. 12 Joint torque trajectories due to the cycling motion

When the pedal position and angle trajectories are given as Fig. 11, joint torque and power trajectories are calculated as Fig. 12 and 13.

3.3 Joint torque for pedal force

While cycling, the foot force is applied to the pedal to drive the crank. This pedal force requires additional joint torques. Given the force F_p(Fig. 14) during the pedal movement, the

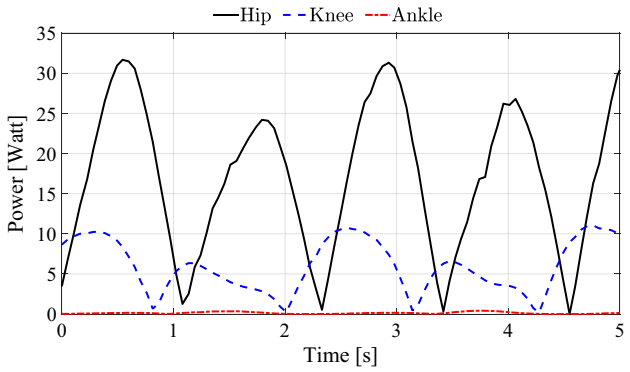

Fig. 13 Absolute joint power trajectories due to cycling motion

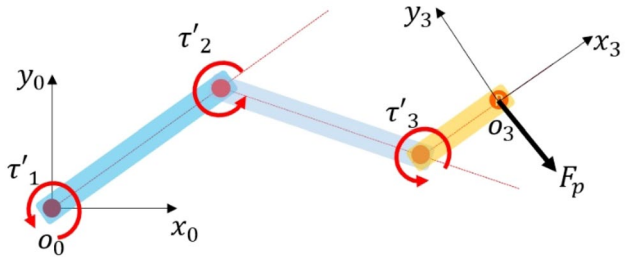

Fig. 14 Additional joint torques for pedal force

necessary additional torque (τ') on each joint can be found using Eq. (37). J^T is the transposed Jacobian matrix (Eq. (38)) and F_p^0(Eq. (39)) is the force vector at the pedal with respect to the base frame at the hip joint. Because our pedal can only measure the normal force, the other forces were assumed to be zero.

$$\tau' = J^T F_p^0 \tag{37}$$

$$J^T = \begin{bmatrix} -L_1 s_1 - L_2 s_{12} - L_3 s_{123} & L_1 c_1 + L_2 c_{12} + L_3 c_{123} & 0 \\ -L_{12} s_{12} - L_3 s_{123} & L_2 c_{12} + L_3 c_{123} & 0 \\ -L_3 s_{123} & L_3 c_{123} & 0 \end{bmatrix} \tag{38}$$

$$F_p^0 = R_3^0 F_p^3 = \begin{bmatrix} c_{123} & s_{123} & 0 \\ s_{123} & c_{123} & 0 \\ 0 & 0 & 0 \end{bmatrix} \begin{bmatrix} 0 \\ -F_p \\ 0 \end{bmatrix} \tag{39}$$

where $c_i = \cos(\theta_i)$, $s_i = \sin(\theta_i)$, $c_{ij} = \cos(\theta_i + \theta_j)$, $s_{ij} = \sin(\theta_i + \theta_j)$, $c_{ijk} = \cos(\theta_i + \theta_j + \theta_k)$, $s_{ijk} = \sin(\theta_i + \theta_j + \theta_k)$, R_3^0 is the rotation matrix between the base frame and the foot frame and F_p^3 is the force vector with respect to the foot frame.

After solving the above equations, we found that the additional torque at each joint can be derived by using Eq. (40).

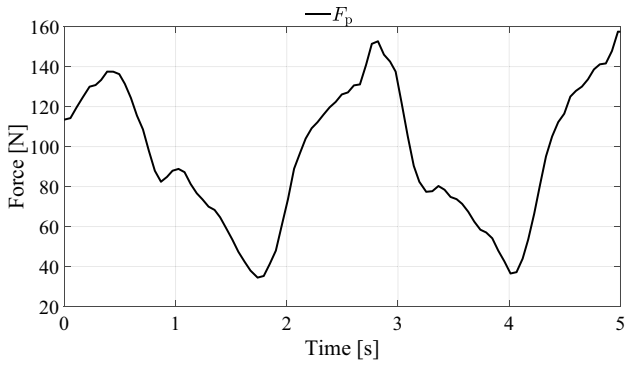

Fig. 15 Example of pedal force trajectory

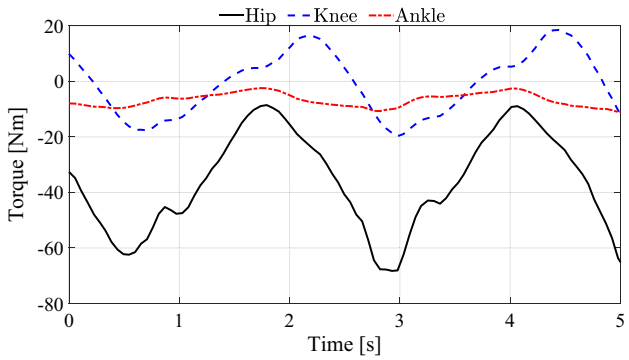

Fig. 16 Additional joint torque trajectories for the pedal force

$$\begin{bmatrix} \tau'_1 \\ \tau'_2 \\ \tau'_3 \end{bmatrix} = \begin{bmatrix} -F_p(L_1 c_{23} + L_2 c_3 + L_3) \\ -F_p(L_2 c_3 + L_3) \\ -F_p L_3 \end{bmatrix} \tag{40}$$

In Figs. 15, 16 and 17, it is seen that the additional joint torque and power trajectories were calculated well from the given pedal force trajectory during the same cycling motion as in Sect. 3.2. The final torque on each joint is the sum of the torque generated by performing the cycling motion and the additional torque for the pedal force. Figure 18 shows the final joint torque trajectories. The absolute power of each joint is calculated in the same manner: it is the sum of cycling motion power and pedal force power (Fig. 19).

4 Power assistance algorithms

In this study, two types of assistive algorithms are proposed to determine the assistive torque. First, the rear wheel torque assistance algorithm is aimed at older adults

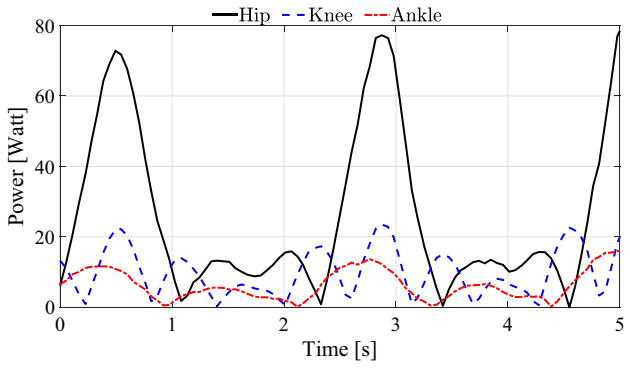

Fig. 17 Additional absolute joint power trajectories for the pedal force

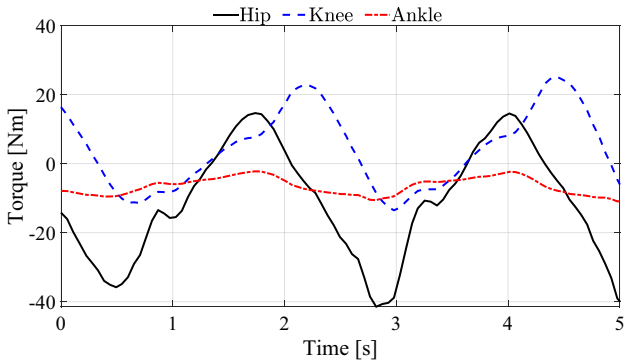

Fig. 18 Final torque trajectories on each joint considering both cycling motion and pedal force

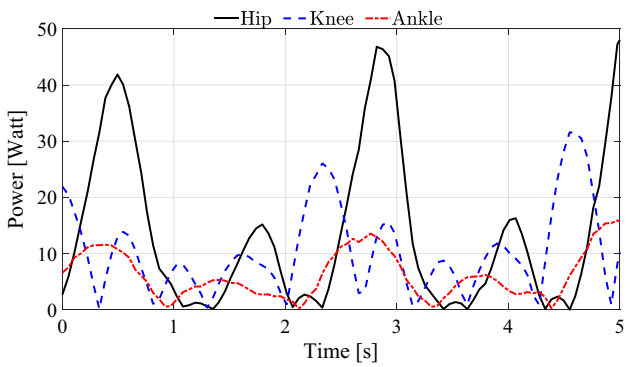

Fig. 19 Final absolute power trajectories on each joint considering both cycling motion power and pedal force power

with weak muscle strength on the lower body, and it focuses on reducing the cyclist's total amount of muscle power necessary to ride the trike (Fig. 20a). On the other hand, the joint torque assistance algorithm is designed to reduce the physical effort of a specific joint of the leg for people with an abnormal joint condition that makes it

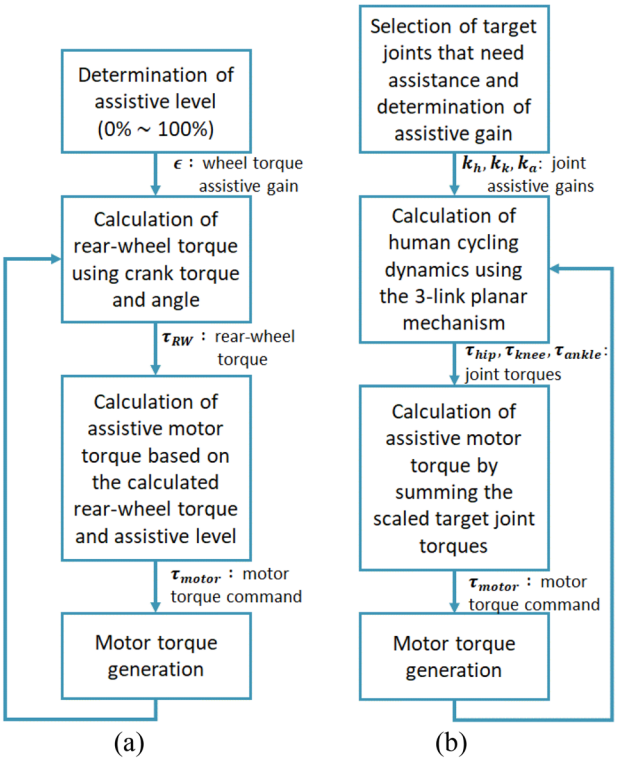

Fig. 20 Flowcharts of the proposed assistive algorithms: **a** Rear-wheel torque assistance, **b** Joint torque assistance

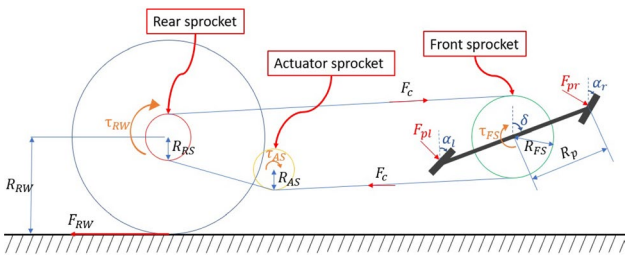

Fig. 21 Trike sprockets schematic

hard for them to cycle without aggravating the preexisting problem (Fig. 20b).

4.1 Relationship between the pedal and the rear-wheel

By analyzing the gear ratio of the trike, it is possible to find important relationships for the assistive algorithms. Figure 21 shows the sprocket schematic of the trike system and Table 3 presents the symbols and dimensions. The first step is to find the crank torque τ_{FS}, due to both pedal forces; this can be done by using the measured pedal forces F_{pr} and F_{pl}, pedal angles α_r and α_l, and crank angle δ. From the schematic of Fig. 22, the right crank torque τ_r

Table 3 Symbol description of sprocket schematics

Symbols	Description
F_c[N]	Tension in the chain
F_{RW}[N]	Rear wheel force
τ_{RW}[Nm]	Rear wheel torque
τ_{AS}[Nm]	Actuator sprocket torque
τ_{FS}[Nm]	Front sprocket torque (=Crank torque)
Data collected from the sensors	
F_{pr}[N]	Force applied to right pedal
F_{pl}[N]	Force applied to left pedal
α_r[deg]	Right pedal angle
α_l[deg]	Left pedal angle
δ[deg]	Crank angle

	Dimensions	Value
R_{RW}[m]	Rear wheel radius	0.6604
R_{RS}[m]	Rear sprocket radius	0.0225
R_{AS}[m]	Actuator sprocket radius	0.0285
R_{FS}[m]	Front sprocket radius	0.0890
R_p[m]	Pedal crank arm distance	0.1700

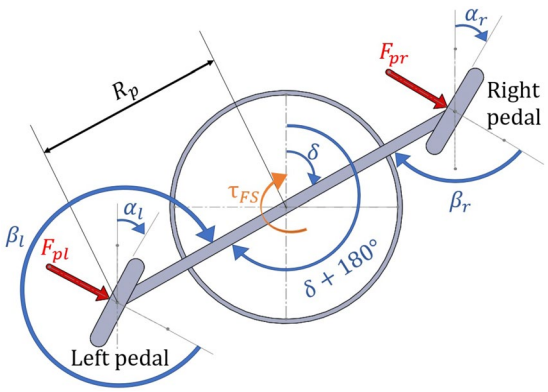

Fig. 22 Front sprocket schematic

due to the right pedal and the left crank torque τ_l due to the left pedal can be found by using the following equations.

$$\tau_r = R_p F_{pr} \sin \beta_r \tag{41}$$

$$\tau_l = R_p F_{pl} \sin \beta_l \tag{42}$$

where

$$\beta_r = \delta + 90° - \alpha_r \tag{43}$$

$$\beta_l = \delta + 270° - \alpha_l \tag{44}$$

The crank torque τ_{FS}, which is the same as the front sprocket torque, is the sum of the right and left crank torques, resulting in Eq. (45).

$$\tau_{FS} = \tau_r + \tau_l \tag{45}$$

Considering the front sprocket as the driver and the rear sprocket as the driven, the relationship between the front and rear sprocket torque is given by Eq. (46).

$$\tau_{RW} = \frac{\tau_{FS} R_{RS}}{R_{FS}} \tag{46}$$

4.2 Rear-wheel torque assistance

The rear-wheel torque assistance algorithm works by relating the rear wheel torque τ_{RW}, with the motor torque τ_{motor}. Because of the harmonic planetary gear of the actuation system, the relationship between the motor torque and the actuator sprocket torque τ_{AS}, is given by Eq. (47). Here, 30 is the reduction ratio of the harmonic planetary gear, η_{gear} is the gear efficiency of 0.9, τ_f is the friction torque of 0.045 Nm from the motor to the harmonic gear, and τ_{motor} is the motor torque.

$$\tau_{AS} = 30\, \eta_{gear} \left(\tau_{motor} - \tau_f \right) \tag{47}$$

Because the actuator sprocket was considered the driver and the rear sprocket was considered the driven, we can derive Eq. (48), which calculates the actuator sprocket torque as a function of the rear wheel torque.

$$\tau_{AS} = \frac{\tau_{RW} R_{AS}}{R_{RS}} \tag{48}$$

By combining Eqs. (47) and (48), it is possible to relate the motor torque with the rear-wheel torque as given in Eq. (49).

$$\tau_{motor} = \frac{\tau_{RW} R_{AS}}{30\, \eta_{gear} R_{RS}} + \tau_f \tag{49}$$

Therefore, we can continuously calculate the rear-wheel torque using Eq. (46) during cycling and then determine the assistive motor torque by using the following equation with an assistive gain.

$$\tau_{motor} = \varepsilon \frac{\tau_{RW} R_{AS}}{30\, \eta_{gear} R_{RS}} + \tau_f \tag{50}$$

In Eq. (50), ε is the wheel torque assistive gain. The motor only works while the rider is pedaling, and the motor is used to reduce the amount of effort from the pilot while cycling. The rear-wheel torque assistive gain, ε, determines how much assistance is given by the motor, where 0 is 0% assistance, i.e., the motor is not working, and 1 is 100% assistance.

4.3 Joint torque assistance

The joint torque assistance algorithm determines the torque of the motor in relation to the joint torques described in Chapter 3. To reduce the specific joint torque during cycling, the motor torque should be determined according to the target joint torque. This means that the assistive motor torque can be proportional to the final joint torque due to cycling motion and pedal force, which is calculated in real-time. Equation (51) shows the assistive motor torque for the final joint torques for a single leg.

$$\tau_{motor} = k_h \left|\tau_{hip}\right| + k_k \left|\tau_{knee}\right| + k_a \left|\tau_{ankle}\right| \tag{51}$$

$$\begin{cases} \tau_{hip} = \tau_1 + \tau_1' \\ \tau_{knee} = \tau_2 + \tau_2' \\ \tau_{ankle} = \tau_3 + \tau_3' \end{cases} \tag{52}$$

where τ_{hip}, τ_{knee}, τ_{ankle} are the final joint torques composed of the torque τ from the cycling motion and the torque τ' from the pedal force, and k_h,k_k, and k_a are, respectively, the joint assistive gains for the hip, knee, and ankle joints. By determining the gain values, it is possible to assist one specific joint or multiple joints. The gains can be heuristically determined depending on the degree of joint assistance desired. The joint torques are also calculated without difficulty according to the passenger's body parameters; hence, the assistive gains act as scaling factors for the absolute joint torques. Although Eq. (51) is for one leg, it can be applied for both legs.

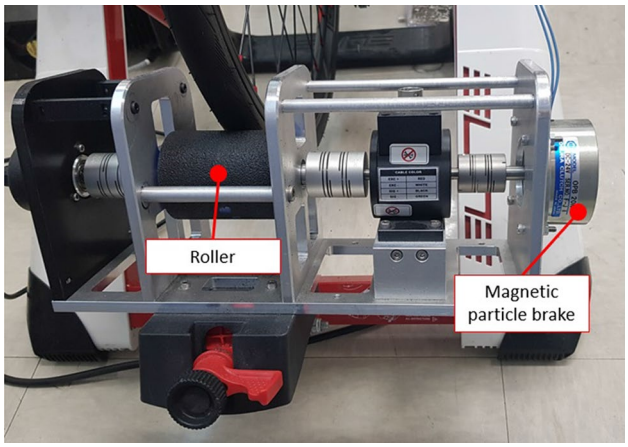

Fig. 23 Developed adjustable brake friction device

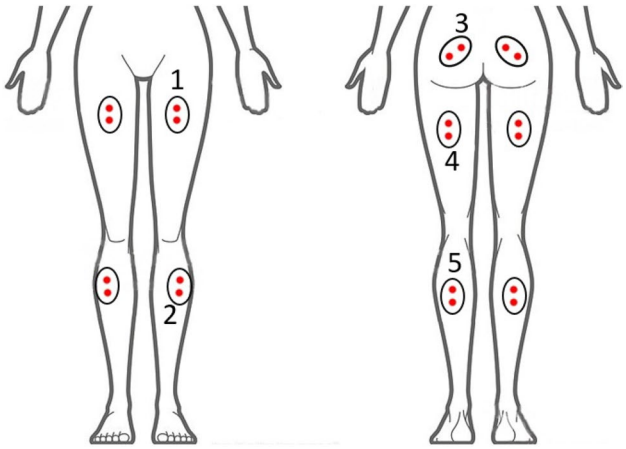

Fig. 24 Location of superficial electrode: (1) RF, (2) TA, (3) GMX, (4) HAM, (5) GAS

5 Experiments

5.1 Experimental setup

The experiments were conducted in the laboratory using an adjustable brake friction device, which was developed in this study, to apply suitable friction torque on the rear wheel. This device can provide a controlled experimental environment with minimal uncertainties that can alter the experiment results. Currently, it is composed of a 24 V magnetic particle brake and a roller (Fig. 23).

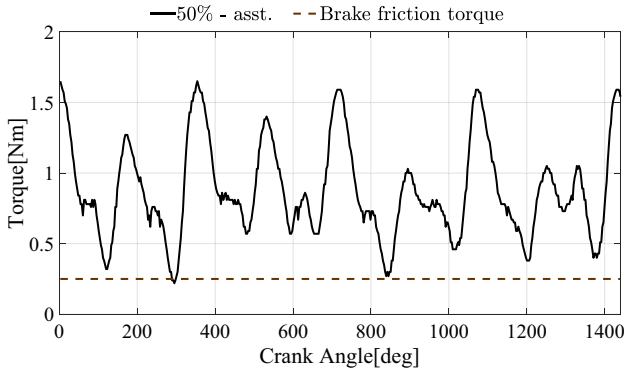

Fig. 25 Actuator torque trajectory for constant brake friction

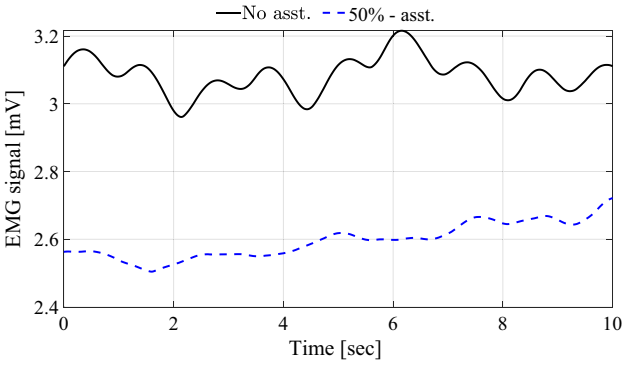

Fig. 27 Average integrated EMG signals for constant brake friction

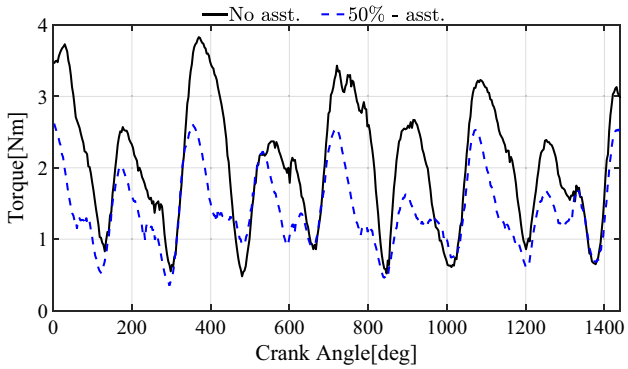

Fig. 26 Calculated rear wheel torque for constant brake friction

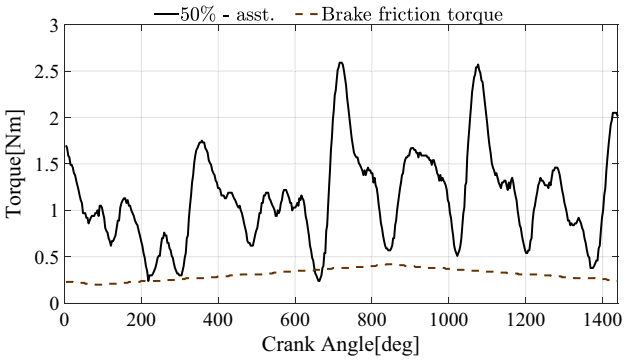

Fig. 28 Actuator torque trajectory for varying brake friction

During experiments, electromyography (EMG) signals were collected from five muscles of the lower limbs that are mainly involved in cycling (Fig. 24): gluteus maximus (GMX), hamstring (HAM), rectus femoris (RF), medial gastrocnemius (GAS), and tibialis anterior (TA). The average integrated EMG values of the five muscles were plotted in each test and RMS values were compared after the experiments. The test subject's average cycling speed during all experiments was 25 RPM.

5.2 Rear-wheel torque assistance test

To verify the rear-wheel torque assistance, we compared the experimental data with and without the motor's assistance [27]. The test subject described in Table 2 conducted this test, and the cycling speed was maintained at 25 RPM in each test. The experiments were done with two different brake friction settings: a constant and a varying friction torque for the roller. The constant brake friction torque was 0.25 Nm, and the varying friction torque changed from 0.20 Nm to 0.42 Nm according to the distance.

The motor's assistance level was set to 50%; ϵ from Eq. (50) hence was 0.5. In the case of 50%-motor assistance with constant brake friction, the actuator torque trajectory is shown in Fig. 25 and the calculated rear-wheel torque trajectory from the pedal force is presented in Fig. 26. In Fig. 26, it can be seen that the calculated rear-wheel torque was reduced with the assistance of the motor at the same speed and friction level. This means that the pedal forces were reduced during cycling. The EMG signal in Fig. 27 was also reduced with motor assistance, compared to cycling without assistance. With the motor's assistance, there was less demand for power from the leg muscles.

When there was assistance from the motor (Fig. 28) for the varying brake friction, wheel torque values (Fig. 29) and the average integrated EMG signals (Fig. 30) were reduced similarly.

Table 4 shows the RMS values for the calculated rear wheel torque and the EMG signal. From this, it is easier to visualize the degree of reduction provided by the motor. The rear-wheel torque was 30% assisted and the EMG signals were reduced by approximately 19% for both cases.

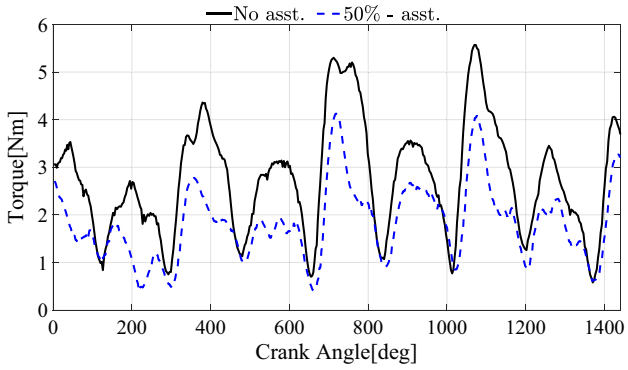

Fig. 29 Calculated rear wheel torque for varying brake friction

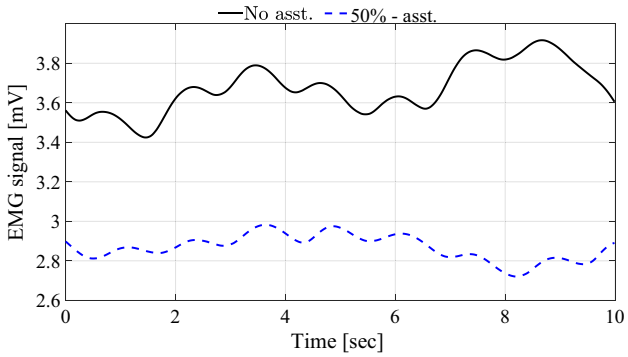

Fig. 30 Average integrated EMG signals for varying brake friction

5.3 Joint torque assistance test

In this section, the joint torque assistance was also verified by comparing the experimental data with and without the assistance of the motor [27]. In particular, in this case, the experimental data from the right and left legs were analyzed separately, because we assumed that the right leg of the rider has a problem; hence, the joints of the right leg were assisted only. Also, for these tests, the same test subject participated, and the cycling cadence was 25 RPM. The experiments were performed with varying friction torque changing from 0.20 Nm to 0.42 Nm according to the distance. Three specific joint assistive experiments were performed: the first was right hip joint assistance only with k_h= 0.01, the second was right knee joint assistance only with k_k= 0.02, and the third was right ankle joint assistance only with k_a= 0.02. The joint assistive gains were experimentally determined, and the joint assistive gains of the joints that were not being assisted were set to zero.

The actuator torque trajectories for the three experiments are presented in Fig. 31. The data from both leg joint torques with and without assistance can be seen in Figs. 32, 33 and 34 and the calculated RMS values are given in Table 5. From these figures, the reductions in the joint torques for both legs are easily noticeable even though only the right leg was assisted. However, when looking at the RMS values in Table 5, the reductions on the right joint torques were two times higher than those on the left joint torques. These results mean that both legs were assisted; however, the assistance of the target leg was sufficiently larger than that for the other leg.

The average integrated EMG data of the five muscles in the right leg were collected for all three joint assistive experiments and compared with the case without assistance (Fig. 35). From the figure, we can easily notice that the EMG signal of the right leg without assistance, compared to all three assisted experiments, was considerably higher. The RMS values of the EMG signals are also summarized in Table 6 with the reduction rate. It can be seen that the muscle activities were substantially reduced, and the reduction rate of the knee joint was the highest.

5.4 Discussion

As shown in the experimental results, there were significant reductions in pedal forces when using the rear-wheel torque assistance method, and also there was a significant reduction in the joint torque for the target leg joint. While

Table 4 RMS values of calculated rear wheel torque and EMG signal at the same speed

1. Constant Friction	No assistance	50%—assisted	Reduction rate [%]
RMS Rear Wheel Torque [Nm]	1.99	1.39	30.20
RMS EMG [mV]	3.08	2.60	15.58
2. Varying Friction	No assistance	50%—assisted	Reduction rate [%]
RMS Rear Wheel Torque [Nm]	2.68	1.83	31.7
RMS EMG [mV]	3.68	2.87	22.01

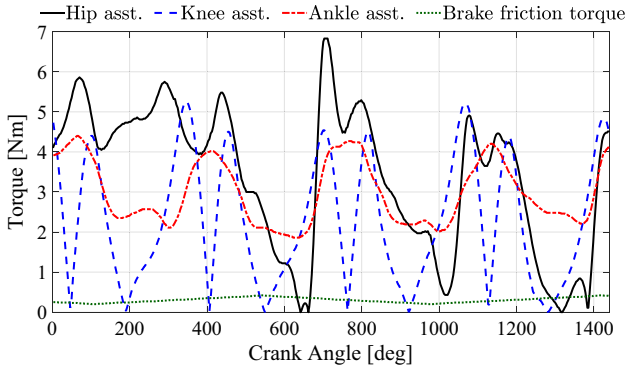

Fig. 31 Actuator torque trajectories of three joint torque assistance tests for varying brake friction

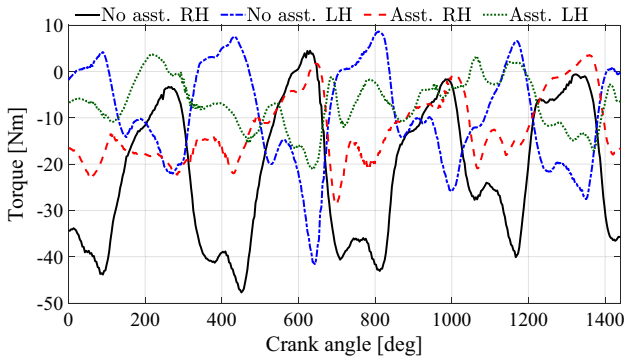

Fig. 32 Hip joint torque trajectories for both legs with and without right hip assistance. RH = right hip; LH = left hip

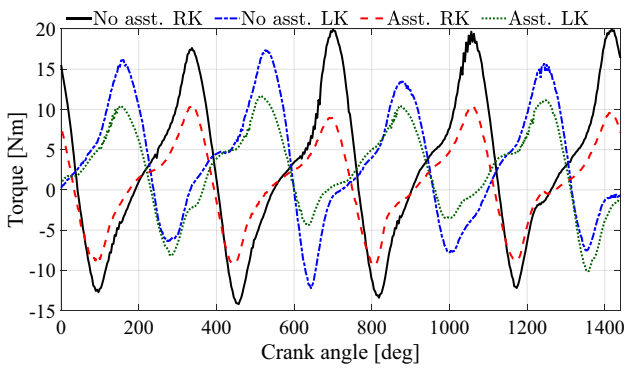

Fig. 33 Knee joint torque trajectories for both legs with and without right knee assistance. RK = right knee; LK = left knee

previous studies have focused on external and environmental parameters to determine the motor's assistive power [22–26], our experimental results demonstrated that it is possible to use the human parameters, conditions, and cycling pattern to provide more personal assistance that can be adjusted by the rider's necessity.

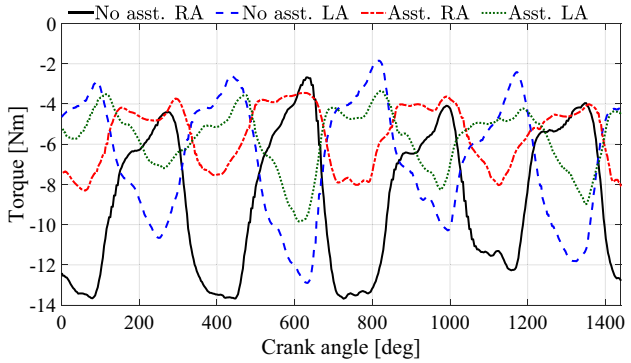

Fig. 34 Ankle joint torque trajectories for both legs with and without right ankle assistance. RA = right ankle; LA = left ankle

There are two things to notice from the results. First, when analyzing the results for the rear-wheel torque assistance method, it is inevitable to notice that the reduction rate for the 50% assistance level was less than 50%. This occurred because this method requires an amount of force being applied to the pedal for the motor to work; hence, even with 100% motor assistance, it would still not be possible to achieve a 100% reduction rate. Second, regarding the joint torque assistance, not only the target leg joint was assisted, but also the joint from the opposite leg got a meaningful reduction. This demonstrates that independent joint assistance is not possible, because when the motor rotates the crank both pedal arms are turned.

6 Conclusion

In this paper, two types of assistive methods for an e-trike were proposed to reduce the muscle power and joint torque required during cycling for older adults who have weak lower body muscles and joint-related problems so that they can participate in helpful physical activities. More specifically, the rear-wheel torque assistance method is to reduce the total amount of muscle power on the lower body, and the joint torque assistance method is to reduce the physical effort of a specific joint of the leg without aggravating the preexisting problem. We built an indoor experiment environment and showed that the experimental results for both assistive methods successfully verified the performances. First, the rear-wheel torque assistive method showed high reductions in the torque (approx. 30%-reduction) of the rear wheel calculated from the pedal forces for the same resistance and speed, as well as in the EMG signal (approx. 19%-reduction) of the legs. Second, the joint torque assistive method was able to reduce the specific joint torque higher than 38% during cycling. It was seen that the joint torque assistance also reduced the torque of

Table 5 RMS values of joints torque trajectories for the three tests

Test	Joint	No assistance [Nm]	Assisted [Nm]	Reduction rate [%]
(1) Hip only asst	Right hip	27.03	13.24	51.02
	Left hip	14.03	10.87	22.51
(2) Knee only asst	Right knee	9.87	5.51	44.17
	Left knee	7.87	5.67	27.93
(3) Ankle only asst	Right ankle	9.63	5.93	38.44
	Left ankle	7.17	6.05	15.55

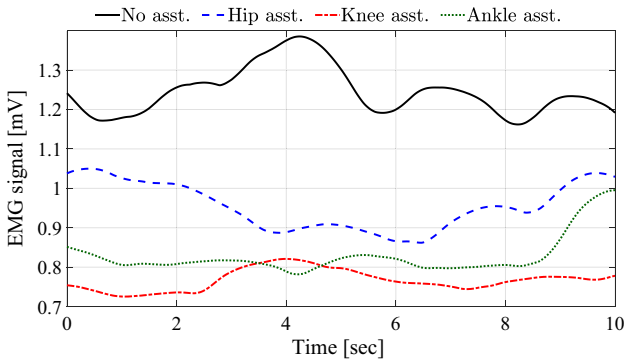

Fig. 35 Averaged integrated EMG signal trajectories for right leg with and without three types of assistance

Table 6 RMS values of EMG signal for the three tests

	RMS EMG [mV]	Reduction rate [%]
No assistance	1.25	
(1) Hip only assistance	0.96	23.34
(2) Knee only assistance	0.77	38.44
(3) Ankle only assistance	0.83	33.65

the same joint of the opposite leg, however, the reduction rates of the joint of the opposite leg were two times lower.

As a result, we believe that the proposed power assistive e-trike can be effectively utilized as a safe rehabilitation or exciting exercise tool for older adults or patients with lower limb disabilities. When older adults use the proposed e-trike outdoor, they will be able to exercise their upper body muscles for steering and train their immediate judgment from visual feedback. Currently, there are many commercial recumbent e-trikes, but they mostly use thumb throttles and do not consider the cyclist's dynamics or joint conditions. Hence, we hope that our study will provide useful insight for developing a recumbent e-trike.

In the near future, we will conduct outdoor cycling experiments after system improvement, and analyze the effectiveness of the proposed method for varying speed and resistance. Consequently, we will verify our algorithms for the older adults and patients by adjusting the assistive gains and body parameters after obtaining an IRB approval. As a long-term study, machine learning algorithms will be applied to automatically determine the suitable assistive gains for individual customization.

Supplementary Information The online version contains supplementary material available at https://doi.org/10.1007/s11370-021-00373-8.

Acknowledgements This study was supported by the Research Program funded by the SeoulTech (Seoul National University of Science and Technology)

References

1. Sharma H, Swami B (2016) Congestion Characteristics of Interrupted Flow for Urban Roads with Heterogeneous Traffic Structure. MATEC Web of Conferences 81:01001. https://doi.org/10.1051/matecconf/20168101001
2. Mihet-Popa L, Saponara S (2018) Toward Green Vehicles Digitalization for the Next Generation of Connected and Electrified Transport Systems. Energies 11:3124. https://doi.org/10.3390/en11113124
3. Panter J, Desousa C, Ogilvie D (2013) Incorporating walking or cycling into car journeys to and from work: The role of individual, workplace and environmental characteristics. Prev Med 56:211–217. https://doi.org/10.1016/j.ypmed.2013.01.014
4. Tolley R (1996) Green campuses: cutting the environmental cost of commuting. J Transp Geogr 4:213–217. https://doi.org/10.1016/0966-6923(96)00022-1
5. Langford B, Cherry C, Bassett D et al (2017) Comparing physical activity of pedal-assist electric bikes with walking and conventional bicycles. J Transp Health 6:463–473. https://doi.org/10.1016/j.jth.2017.06.002
6. Ratey J, Loehr J (2011) The positive impact of physical activity on cognition during adulthood: a review of underlying mechanisms, evidence and recommendations. Rev Neurosci. https://doi.org/10.1515/rns.2011.017
7. Lau H, Mat Ludin A, Rajab N, Shahar S (2017) The association between physical fitness with successful ageing and risk of cognitive impairment among Malaysian older adults. J Sains Kesihatan Malaysia 15:97–102. https://doi.org/10.17576/jskm-2017-1502-13
8. Van Cauwenberg J, De Bourdeaudhuij I, Clarys P et al (2018) Older E-bike users. Med Sci Sports Exerc 50:1780–1789. https://doi.org/10.1249/mss.0000000000001638
9. Leyland L, Spencer B, Beale N et al (2019) The effect of cycling on cognitive function and well-being in older adults. PLoS ONE 14:e0211779. https://doi.org/10.1371/journal.pone.0211779

10. Gomes G, Teixeira-Salmela L, Freitas F et al (2016) Gait performance of the elderly under dual-task conditions: Review of instruments employed and kinematic parameters. Revista Brasileira de Geriatria e Gerontologia 19:165–182. https://doi.org/10.1590/1809-9823.2016.14159
11. Nascimento, M (2019) Fall in older adults: Considerations on balance regulation, postural strategies, and physical exercise. 13: 1–12. doi:https://doi.org/10.5327/Z2447-211520191800062
12. Sakurai R, Kawai H, Suzuki H et al (2019) An epidemiological study of the risk factors of bicycle-related falls among japanese older adults. J Epidemiol 29:487–490. https://doi.org/10.2188/jea.je20180162
13. Wellsandt E, Golightly Y (2018) Exercise in the management of knee and hip osteoarthritis. Curr Opin Rheumatol. https://doi.org/10.1097/bor.0000000000000478
14. Guralnik M, Ferrucci L et al (1995) Lower-extremity function in persons over the age of 70 years as a predictor of subsequent disability. N Engl J Med. https://doi.org/10.1056/nejm199503023320902
15. Rampazo-Lacativa K, D'Elboux J (2015) Effect of cycle ergometer and conventional exercises on rehabilitation of older patients with total hip arthroplasty: study protocol for randomized controlled trial. Trials. https://doi.org/10.1186/s13063-015-0647-8
16. Macaluso A, Young A et al (2003) Cycling as a novel approach to resistance training increases muscle strength, power, and selected functional abilities in healthy older women. J Appl Physiol. https://doi.org/10.1152/japplphysiol.00416.2003
17. Mujika I, Rønnestad R, Martin T (2016) Effects of increased muscle strength and muscle mass on endurance-cycling performance. Int J Sports Physiol Perform. https://doi.org/10.1123/ijspp.2015-0405
18. So H, Ng K-F, Ng F (2005) Muscle recruitment pattern in cycling: a review. Phys Ther Sport. https://doi.org/10.1016/j.ptsp.2005.02.004
19. Savelberg M, Van de Port L, Willems B (2003) Body configuration in cycling affects muscle recruitment and movement pattern. J Appl Biomech. https://doi.org/10.1123/jab.19.4.310
20. Yamazaki H, Matsuda A (2016) Joint torque evaluation of lower limbs in bicycle pedaling. Procedia Eng. https://doi.org/10.1016/j.proeng.2016.06.275
21. Wangerin M, Schmitt S, Stapelfeldt B, Gollhofer A (2007) Inverse dynamics in cycling performance. Adv Med Eng. https://doi.org/10.1007/978-3-540-68764-1_55
22. Guarisco M, Gao F, Paire D (2017) Autonomy and user experience enhancement control of an electrically assisted bicycle with dual-wheel drive. IEEE Trans Ind Appl 53:1476–1484. https://doi.org/10.1109/tia.2016.2617299
23. Abagnale C, Cardone M, Iodice P et al (2016) Design and Development of an Innovative E-Bike. Energy Procedia 101:774–781. https://doi.org/10.1016/j.egypro.2016.11.098
24. Lee J, Jiang J (2019) Enhanced fuzzy-logic-based power-assisted control with user-adaptive systems for human-electric bikes. IET Intel Transport Syst. https://doi.org/10.1049/iet-its.2019.0092
25. Abhilash D, Wani I et al (2019) Power efficient e-bike with terrain adaptive intelligence. Int Conf Commun Electron Syst (ICCES). https://doi.org/10.1109/ICCES45898.2019.9002178
26. Huang C, Dai B, Yeh T (2018) Determination of motor torque for power-assist electric bicycles using observer-based sensor fusion. J Dyn Syst Meas Contr. https://doi.org/10.1115/1.4039280
27. Rosa T [HRRLAB On Air] (2020, October 19) Power Assistance Algorithm of an E-trike Based on Inverse Dynamics for Older Adults [Video file] Retrieved from https://www.youtube.com/watch?v=-ToPHNnAAx0&t=54s